Icarus 378 (2022) 114934

Contents lists available at ScienceDirect

Icarus

journal homepage: www.elsevier.com/locate/icarus

Constraints on the uncertainty, timing, and magnitude of potential Mars oceans from topographic deformation models

Steven F. Sholes [a,*], Frances Rivera-Hernández [b]

[a] Jet Propulsion Laboratory, California Institute of Technology, 4800 Oak Grove Dr, Pasadena, CA 91109, United States of America
[b] Georgia Institute of Technology, Department of Earth and Atmospheric Sciences, 311 Ferst Dr, Atlanta, GA 30332, United States of America

ARTICLE INFO

Keywords:
Mars
Oceans
Shorelines
Tharsis
Habitability

ABSTRACT

Proposed ocean paleoshorelines on Mars have faced criticism over their genetic interpretation and because they deviate significantly from an expected equipotential surface (by many kilometers). Multiple geophysical deformation models have been proposed to explain this large topographic range and deviation including true polar wander and direct Tharsis-induced deformation. Yet, the application of these models is potentially flawed as there exists no consensus on exactly where these proposed paleoshorelines are located. Here, we apply these models to proposed maps and mappings of the putative martian ocean shorelines and show that even when considering deformation due to the rise of Tharsis and its associated true polar wander, the observed deviation within each Arabia level's paleotopography precludes them as past equipotential surfaces. Additionally, we compute best-fit ages for all proposed paleoshorelines relative to the rise of Tharsis and the ages span nearly the entire period of Tharsis construction. Assessment of the paleoelevations of open basin deltas and valley network termini also suggests disagreement with the timing of such features with a paleoocean. Overall, we find that these geophysical deformation models are unable to explain the large elevation ranges observed in the putative shoreline data and that the long-wavelength trends may simply be the result of mismapped features along the topographic dichotomy which itself may have been modified by Tharsis and/or true polar wander.

1. Introduction

Evidence for past oceans on Mars has long been a controversial topic (Dickeson and Davis, 2020). The most compelling evidence for early martian oceans is proposed paleoshorelines that encircle the northern plains of Mars (Parker et al., 1993; Parker et al., 1989; Zuber, 2018). These hypothesized ocean paleoshorelines have faced considerable scrutiny over their genetic interpretations (Carr and Head, 2003; Ghatan and Zimbelman, 2006; Malin and Edgett, 1999; Sholes, 2019; Sholes et al., 2019), mainly because they do not follow equipotential surfaces, a characteristic property of ocean margins (Carr and Head, 2003). Yet, understanding the validity of these hypothesized paleoshorelines is crucial for evaluating whether Mars ever had oceans, and constraining Mars' past water budget, climate, and potential for habitability.

The two main proposed ocean paleoshorelines on Mars are referred to as the Arabia and Deuteronilus Levels (Contacts 1 and 2 respectively in the older literature). The Arabia Level approximately follows the topographic dichotomy and has been hypothesized to represent a large early erosional ocean stand. The Deuteronilus Level generally follows the southern boundary of the Vastitas Borealis Formation (VBF) and has been hypothesized as the depositional remnants of a Hesperian-aged ice-covered ocean (Carr and Head, 2019; Clifford and Parker, 2001; Parker et al., 1993; Parker et al., 2010; Parker et al., 1989). Additionally, observations have suggested that these levels correspond with the termination of valley networks/outflow channels (Clifford and Parker, 2001; Parker et al., 1993; Parker et al., 1989) and in mean elevation with open basin deltas along the crustal dichotomy (Di Achille and Hynek, 2010). Although, subsequent detailed regional mapping has shown that many of these deltas likely formed in closed localized paleolakes or seas rather than a northern ocean (Davis et al., 2021; De Toffoli et al., 2021; García-Arnay and Gutiérrez, 2020; Rivera-Hernandez and Palucis, 2019).

The Arabia and Deuteronilus Levels span multiple kilometers in elevation over their length, both in their long-wavelength (global) and short-wavelength (10s of degrees longitude) trends (Fig. 1). Detailed

Abbreviations: TID, Tharsis-induced deformation; TPW, true polar wander; VBF, Vastitas Borealis Formation; MOLA, Mars Orbiter Laser Altimeter; HRSC, High Resolution Stereo Camera; DEM, digital elevation model; CTX, Context Camera; GEL, global equivalent layer.

* Corresponding author.
E-mail address: steven.f.sholes@jpl.nasa.gov (S.F. Sholes).

https://doi.org/10.1016/j.icarus.2022.114934
Received 17 September 2021; Received in revised form 29 January 2022; Accepted 1 February 2022
Available online 5 February 2022

analysis of the Mars Orbiter Laser Altimeter (MOLA; Smith et al., 2001) elevation data by Carr and Head (2003) and Head et al. (1999) found that the Arabia Level has a total topographic range exceeding 5.8 km along its length (mean elevation of −2.09 ± 1.4 km) while the Deuteronilus Level spans a total of 1.2 km (mean elevation of −3.79 ± 0.24 km) in elevation. More recent detailed mapping of the Deuteronilus Level by Ivanov et al. (2017) found that it better fit two distinct levels of −3.91 ± 0.08 km and −3.58 ± 0.09 km with topographic ranges of 0.94 km and 1.11 km respectively (excluding the Tantalus, Phlegra, and Isidis regions). The Arabia Level, unlike the Deuteronilus Level which largely follows an observable geological contact (the VBF), is diffuse and exhibits different morphologies, thus a published detailed geological map for the Arabia Level does not currently exist (Sholes et al., 2021).

There are multiple scenarios that may explain these large topographic differences with each proposed paleoshoreline level: 1) the misidentification of features as genetically paleoshorelines (Carr and Head, 2003; Clifford and Parker, 2001; Sholes, 2019; Sholes et al., 2014), 2) errors resulting from mismapping the proposed paleoshoreline data (Sholes et al., 2021), or 3) topographic deformation after emplacement of the proposed paleoshorelines (Citron et al., 2018; Perron et al., 2007). Multiple geophysical deformation models have been proposed to explain why the mapped levels do not follow an equipotential surface. Early models invoked isostatic rebound (Leverington and Ghent, 2004), thermal isostasy (Ruiz et al., 2004), and mantle plumes (Roberts and Zhong, 2004) to partially explain the observed topographic offsets. Subsequent modeling work has proposed that either true polar wander (TPW; Perron et al., 2007) or deformation due to the uplift of the Tharsis volcanic province (Tharsis-Induced Deformation, TID; Citron et al., 2018) may explain the observed long-wavelength topographic deviations from an equipotential surface (Fig. 1).

However, both models are potentially problematic in their applications for several reasons. Firstly, it is unknown how these models would fit all of the Arabia Level segments. Each model was only applied to a relatively small segment (~100° longitude in Arabia Terra) of the globally-mapped Arabia Level, as it was the longest continuous segment in the Carr and Head (2003) digitization of the Clifford and Parker (2001) map. This approach was taken to avoid assumptions on whether the disjointed mapped Arabia Level segments represented the same formational timing and/or processes.

Secondly, the exact Arabia Level location is unknown. Updated regional mapping by Sholes et al. (2021) showed that large portions of the smaller Arabia Terra segment varied by up to 500 km in its location from the original definition of the level as presented in Parker et al. (1989). This discrepancy in the location of the Arabia Level may be due to its diffuse geomorphic nature, lack of detailed mapping, and/or multiple factors in data propagation (e.g., figure digitization error, smoothing and extrapolating over complex landforms, and redrawing based on new interpretations). Regardless of the reason, mappings for the Arabia Level location vary by an average of 141 ± 142 km in its lateral placement globally which leads to a spread of 2.2 km in mean elevations (Sholes et al., 2021). Thus, which Arabia Level definition is chosen can drastically affect the robustness of deformation model results. The choice of level definition also effects how we interpret and place other possible coastal features into context. For example, open basin deltas along the dichotomy were interpreted by Di Achille and

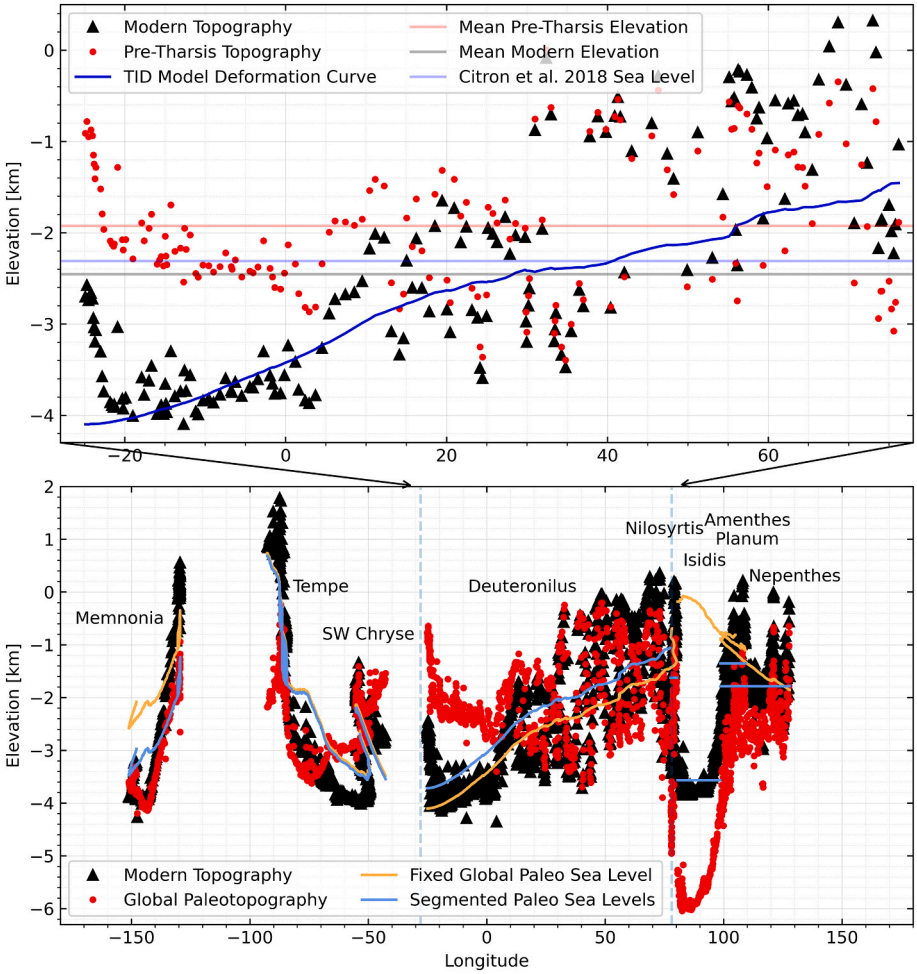

Fig. 1. Comparisons of the modern and paleotopography of the Citron et al. (2018) Tharsis-induced deformation model. *Top*) Replication of the model using the same segment of the Arabia Level. Blue curve indicates best-fit model deformation curve: $C = 1$, $Z = -2.3$ km. Note that the data are plotted versus longitude rather than distance along the feature. *Bottom*) Application of the model to the entire Carr and Head (2003) Arabia Level map. Orange curves are the best-fit model for the entire dataset ($C = 0.61$, $Z = -2.53$ km) corresponding to the pre-Tharsis paleotopography (red dots) while blue curves are best-fit to each named segment (see Table 1). (For interpretation of the references to colour in this figure legend, the reader is referred to the web version of this article.)

Hynek (2010) to closely match the mean elevation of the Arabia Level as defined by Clifford and Parker (2001), but it is unclear how their results fit into other Arabia shoreline definitions.

Thirdly, the TPW model depends on the localization of each level. This is because the TPW model does not rely on any observational evidence for the nominal true polar wander itself, but rather calculates a best-fit paleopole location by minimizing the digitized data elevation variations of each level (Perron et al., 2007). This is in contrast to the TID model in which topographic corrections are a direct result of the uplift of Tharsis, and independent of level localization (Citron et al., 2018). The TID model, however, is still unable to fit data within each mapped level, particularly in the circum-Tharsis region, which may suggest limitations of the model or a requirement to include additional formational and/or isostatic processes (Citron et al., 2019; Citron et al., 2021).

Here we reevaluate the applications of geophysical deformation models in explaining the large observed topographic variability of the proposed martian paleoshorelines. Specifically, we apply the TID model to different mapped definitions of the Arabia and Deuteronilus levels to characterize: 1) whether the paleotopography of each level actually represents an equipotential surface, 2) how choice of mapped level affects the water volume and timing of any potential paleooceans, and 3) how the paleotopography of proposed paleoocean deltas and valley network termini correspond to the different levels. These results are used to specify the uncertainty regarding applications of these models and their limitations in explaining the observed topographic offsets in the putative paleoshorelines.

2. Geophysical deformation models

2.1. True polar wander

In the true polar wander (TPW) model, sufficient internal or surface loading can cause a shift in a planet's orientation relative to its rotational pole, bringing the load closer to the equator. This shift leads to the formation of a new equatorial bulge, flattening the planet, and results in mass redistribution from the paleoequatorial rotational bulge to the new resulting equatorial bulge, thus deforming the surface topography including any potential paleoshorelines that may have been emplaced. The amplitude of this response at a set colatitude (θ) and longitude (φ) is given by:

$$\Delta T_{TPW}(\theta,\varphi) = \frac{\omega^2 a^2}{2g}\left[cos^2\gamma - cos^2\theta\right]\left[h_2 - (1+k_2)\right] \quad (1)$$

Here, ω is the planet's rotation rate, a is the mean planetary radius, g is the surface gravity, and γ is the angular distance between the given point (θ, φ) and the paleopole. The secular degree-2 tidal Love numbers, h_2 and k_2, that depend on the density and elastic structure of Mars (Sohl and Spohn, 1997) can be calculated as a function of assumed lithospheric thickness, T_e (Bouley et al., 2016; Perron et al., 2007).

To assess the deformation magnitude required to explain the observed topographic range of the hypothesized paleoshorelines, the Perron et al. (2007) TPW model scenario minimized the misfit between the observed modern elevation range and the predicted topographic response for each of their tested paleoshoreline levels. The Arabia and Deuteronilus Levels (both segments of the Carr and Head (2003) map which was digitized and interpolated from Clifford and Parker (2001)) had best-fit paleopoles approximately 90° from the center of the Tharsis rise.

However, for loading and unloading of oceans to cause large enough TPW themselves, Tharsis would need to have formed near the polar regions, which opposes most gravitational evidence suggesting it formed near the equator (Bouley et al., 2016; Daradich et al., 2008; Matsuyama and Manga, 2010; Melosh, 1980; Roberts and Zhong, 2007; Willemann, 1984). As surface mass loads would be insufficient to counteract the effects of a near-equatorial Tharsis rise, Perron et al. (2007) invokes internal mass loading, such as from mantle convection, to drive the necessary TPW.

Perron et al. (2007) tested lithospheric thickness values, T_e, of 100–400 km, finding that larger T_e values had better model fits for the tested Arabia Level segment. Their focus was predominantly on a T_e of 200 km, citing modern estimates for Mars' lithospheric thickness (Banerdt et al., 1992; Roberts and Zhong, 2004; Sohl and Spohn, 1997). However, the high-degree of short-wavelength scatter contributed to large root-mean-scatter errors for all values of T_e. This uncertainty from the scatter and opposing fits for T_e values suggests that there is not one preferred T_e value.

The TPW model results from Perron et al. (2007) as a whole implies that both the Arabia and Deuteronilus Levels are younger than the Tharsis rise. Tharsis would resist reorientation of the planet that would move itself away from the equator, constraining any TPW to a great-circle 90° from the gravitational center of the Tharsis rise. The best-fit paleopoles for the Arabia and Deuteronilus Levels are located 86° and 89°, respectively, from the center of Tharsis suggesting both postdate Tharsis (and were deformed from non-Tharsis TPW), which initiated >3.7 Gyr ago (Anderson et al., 2001; Carr and Head, 2010). This claim is further supported by observations of sections of both levels following the margins of the Olympus Mons aureole (Perron et al., 2007). However, geomorphic evidence of the Arabia Level suggests it is older than, or at least coincident with, Tharsis (Clifford and Parker, 2001). Furthermore, these circum-Olympus segments have largely been disregarded as shoreline contacts and generally interpreted as singularly volcanic (Carr and Head, 2003; Malin and Edgett, 1999; Parker et al., 2010).

2.2. Tharsis-induced deformation

The Tharsis-induced deformation (TID) model assumes that the uplift due to the formation of Tharsis itself would deform any possible shorelines. As Tharsis grew, the loading on Mars changes its shape and geoid, creating a local high around Tharsis, a corresponding antipodal bulge, and a circum-Tharsis trough (Cattermole, 1992).

Unlike the TPW model, the TID model is independent of the location of the proposed paleoshoreline and, rather, relies on the observed contributions of Tharsis to Mars' shape. These global topographic contributions to Mars' shape and geoid from the growth of Tharsis were modeled in Matsuyama and Manga (2010) using measured martian gravity field data. Thus, the amplitude of Tharsis-induced deformation at a set colatitude (θ) and longitude (φ) is approximated by:

$$\Delta T_{TID}(\theta,\varphi) = C(\Delta T_{TPW}(\theta,\varphi) + S_{Tharsis}(\theta,\varphi) - N_{Tharsis}(\theta,\varphi)) \quad (2)$$

Here ΔT_{TPW} is the component of any true polar wander that results from Tharsis' formation following Eq. (1), $S_{Tharsis}$ and $N_{Tharsis}$ are the contributions from Tharsis to the shape and geoid of Mars respectively with their coefficients modeled in Matsuyama and Manga (2010) up to degree-5 spherical harmonics (see also Baum et al., 2021 for full spherical harmonics expression). C is a scalar corresponding to the percentage of Tharsis built up after the proposed shoreline's emplacement. Here we scale all terms by the singular parameter C as an approximation of the timing effect of Tharsis' deformation and resulting TPW, but these processes may not scale in the same way. However, as Tharsis likely formed near the equator, the induced TPW component is orders of magnitude smaller than the surface deformation caused directly by the growth of Tharsis (10s of m vs. 1000s of m), so any differences would be minor.

The timing of level formation does require minimizing the topographic offset between the modern level elevations and their paleoelevations for values of C (percentage of Tharsis emplacement after feature formation). Thus, the fidelity of the model to determine the relative ages of the paleoshoreline levels and their long-wavelength trends relies on the accuracy of the mapped levels used. The Citron et al. (2018) study used the same Arabia Level data as in Perron et al.

(2007) but used the improved map of the Deuteronilus Level from Ivanov et al., 2017.

The Arabia Level was found to have a smallest root-mean-square error ($\sigma_{r.m.s.}$) of 590 m corresponding to if 80% of Tharsis was emplaced after the formation of the putative shoreline. However, the authors found a similar error of 615 m if 100% of Tharsis topography was formed after the level formation. Given the errors associated with the short-wavelength scatter in the data and comparable errors to the TPW model in Perron et al. (2007), these results suggest that an early Arabia Level ocean would have formed prior to or during the very early stages of the rise of Tharsis, countering the opposing timeline of the TPW model.

The Deuteronilus Level had the smallest $\sigma_{r.m.s.}$ of 110 m corresponding to the last 17% of Tharsis emplacement, suggesting that the putative paleoshoreline formed during the late stages of Tharsis' growth. However, the model was applied to the entire data set concurrently whereas the cited data suggested, based off applications of the TPW model, that the Deuteronilus Level data is better fit by two different formational events (Ivanov et al., 2017).

3. Methods

3.1. Modeling proposed paleoshoreline levels

We use the Tharsis-induced deformation model as presented in Citron et al. (2018) in our topographic analysis of martian paleoshoreline levels. We chose this model as it does not rely on the mapped level locations, is grounded on observational gravity field data, and performs better at minimizing the root-mean-square error than the TPW model (see Section 2). This model includes contributions both from Tharsis uplift and subsequent induced true polar wander (Fig. 1; Eq. (2)). The model was applied to the Deuteronilus Level (Ivanov et al. (2017) and the differently mapped versions of the Arabia Level (Carr and Head, 2003; Clifford and Parker, 2001; Parker et al., 1993; Parker et al., 2010; Parker et al., 1989; Sholes et al., 2021; Webb, 2004) which includes the smaller Arabia Terra segment used in Perron et al. (2007) and (Citron et al., 2018). Considering all of the different mapped Arabia levels is necessary because there is neither a standardized geospatial dataset nor definition for the Arabia Level which has led to >500 km of lateral offset between the vector data used in the Perron et al. (2007) and Citron et al. (2018) studies with the original geomorphic contact described in Parker et al. (1989) (Sholes et al., 2021).

Both the TPW and TID models contain an additive term for the mean paleosea level, Z, which essentially is a vertical offset that best aligns the modeled topographic correction with the modern topography of the paleoshoreline levels. This value can either be fixed at a specific assumed paleosea level, calculated as the mean paleoelevation of all tested points, or optimized to provide the best fit with the features. Here, we assume that it does represent the paleosea level and is calculated as the mean pre-deformation elevation. Modern elevation data is obtained from the MOLA/HRSC (High Resolution Stereo Camera; Jaumann et al., 2007) blended digital elevation model (DEM) at 200 m/px (Fergason et al., 2018).

However, the discontinuous segments of each mapped level may represent regions emplaced at different times and/or by different formational processes. Thus, we fit the topographic deformation model with both a globally calculated mean paleosea level, hereafter referred to as a global sea level fit, but also by fitting a mean paleosea level to each continuous segment. This allows for both characterization of the paleotopography of the levels and the identification of sections that may differ substantially from the rest of the level.

We do not perform optimization procedures on the various levels to obtain best fit parameter values (e.g., T_e and paleopole location) that minimize the topographic misfit based on physical properties of Tharsis. Instead, we assume standardized parameter values following estimates expected during Tharsis' emplacement: $T_e = 58$ km, $k_2 = 2.0$, $h_2 = 1.1$, and a paleopole location at 259.5°E and 71.1°N (Bouley et al., 2016; Citron et al., 2018). To assess the timing of the putative shorelines, we present both the nominal model results (assuming 100% of Tharsis was emplaced for Arabia, $C = 1$, and 17% of Tharsis was emplaced for Deuteronilus, $C = 0.17$) as well as perform optimization to retrieve the best fit scenarios both globally and segmented.

Additionally, one of the limitations of the Citron et al. (2018) Tharsis-induced deformation model is that the nominal model is inadequate in fitting the paleotopography in the circum-Isidis basin region. A proposed updated model using degree-50 spherical harmonics which incorporates 3 km of loading in Isidis Planitia (Evans et al., 2010; Ritzer and Hauck II, 2009) is being developed (Citron et al., 2019). However, here we use the nominal degree-5 spherical harmonic model and present the results with and without the sections around Isidis (which here we define as from 77° to 99°E for simplicity) for comparison.

3.2. Modeling valley networks and delta elevations

In addition to modeling paleoshoreline levels, we also modeled the paleoelevations of martian deltas and valley networks interpreted by previous studies to have formed in a northern global ocean (Chan et al., 2018; Di Achille and Hynek, 2010). For the valley networks, we used the termini elevations from Chan et al. (2018) which they determined using the global MOLA elevation data (Smith et al., 2001). These valley networks are located in Noachian-aged terrain and originally mapped by Hynek et al. (2010). The mean elevation of the valley network termini is -1.70 ± 0.81 km with a range of 4.18 km.

For the dichotomy deltas, we updated the Di Achille and Hynek (2010) open basin delta inventory by incorporating results from Rivera-Hernandez and Palucis (2019). Here, open basin deltas are defined as those deltas along the topographic dichotomy with paleowater level contours open to the northern lowlands (Di Achille and Hynek, 2010). Of the 50 fan-shaped landforms investigated by Rivera-Hernandez and Palucis (2019) in the Gale crater region, 11 correspond to features interpreted as open basin deltas by Di Achille and Hynek (2010) and 5 new open basin deltas were identified. The basin classification of 7 of these deltas was reinterpreted by Rivera-Hernandez and Palucis (2019) using higher resolution CTX (Context Camera; Malin et al., 2007) and MOLA/HRSC elevation data. With the updated classifications and delta front elevations, the mean elevation of the open basin deltas is -2.29 ± 0.43 km ($N = 17$, range of 1.38 km), in contrast to the mean elevation of -2.54 ± 0.18 km (N = 17, range of 0.65 km) from (Di Achille and Hynek, 2010) (Table 1). Neither the original or updated mean delta elevation values represent a global equipotential surface. The vertical disparity in delta elevation values may be due to the deltas forming in distinct water bodies or to post-depositional deformation.

4. Results

4.1. Arabia level

For the small 100 km Arabia Level segment in Arabia Terra (Perron et al., 2007), modeling results suggest that the topographic deformation curve roughly follows long-wavelength elevation trends (Fig. 1), reproducing Citron et al. (2018) results. However, plotting the best-fit paleotopography of the proposed paleoshoreline shows the large topographical range and uncertainty still present in the data. For this segment, the modern elevation range is 4.4 km and lowers to 3.4 km after subtracting the Tharsis rise contributions. Whereas the mean elevation and standard deviation decrease from -2.45 ± 1.23 km to -1.92 ± 0.74 km. Thus, neither the modern- nor paleotopography of the Arabia Terra segment constitute an equipotential surface (Table 1). The westernmost portions of the segment diverge drastically from the modeled topography (due to the circum-Tharsis trough in the model) while the easternmost portions have a large elevation scatter with most points being ~1 km above the deformation curve (Fig. 1).

Table 1
Summary of modern and best-fit paleoelevation data for the Arabia and Deuteronilus Levels and other landforms. GEL is the global equivalent layer of water corresponding to the volume of such an ocean. [NI] Indicates the data without the circum-Isidis data points (defined here as 77° to 99°E).

	Data	Modern			Paleo			C	GEL [m]
		Mean elevation [km]	Standard deviation [km]	Range [km]	Mean elevation [km]	Standard deviation [km]	Range [km]		
Arabia Level	Parker et al., 1989	−1.94	1.26	5.50	−1.94	1.19	5.69	0.36	570
	Parker et al., 1989[NI]	−1.84	1.24	5.50	−1.69	0.99	5.53	0.74	600
	Parker et al., 1993	−1.52	1.55	7.72	−1.82	1.15	7.24	0.77	540
	Parker et al., 1993[NI]	−1.49	1.56	7.72	−1.77	1.09	5.29	0.84	560
	Clifford and Parker, 2001	−2.23	1.25	6.86	−2.19	1.07	7.14	0.57	450
	Clifford and Parker, 2001[NI]	−2.19	1.25	6.86	−2.07	0.95	5.96	0.75	460
	Carr and Head, 2003	−2.31	1.30	6.13	−2.53	1.11	5.71	0.61	340
	Carr and Head, 2003[NI]	−2.23	1.31	6.13	−2.39	0.84	4.21	0.95	350
	Webb, 2004	−3.72	0.18	0.98	−3.47	0.18	0.98	0.16	170
	Perron et al., 2007	−2.45	1.23	4.42	−1.92	0.74	3.40	1.00	500
	Parker et al., 2010	−3.61	0.26	1.75	−3.14	0.21	1.60	0.46	200
	Sholes et al., 2021	−3.56	0.08	0.36	−3.21	0.06	0.34	0.52	180
Carr and Head 2003 Sections	Memnonia	−2.84	1.51	4.83	−3.20	0.89	3.25	1.00	170
	Tempe	−1.50	1.92	5.72	−2.36	0.84	3.38	1.00	350
	Chryse	−2.96	0.72	2.67	−2.37	0.41	1.74	1.00	350
	Deuteronilus	−2.48	1.19	4.71	−1.92	0.77	3.69	1.00	500
	Nilosyrtis	−1.62	1.05	3.63	−1.62	1.05	3.63	0.00	770
	Isidis	−3.56	0.27	1.32	−3.56	0.27	1.32	0.00	180
	Amenthes	−1.35	0.66	3.12	−1.35	0.66	3.12	0.00	880
	Nepenthes	−1.78	0.54	2.97	−1.78	0.54	2.97	0.00	710
Ivanov et al., 2017 Sections	Deuteronilus Level Global	−3.79	0.20	1.26	−3.68	0.11	1.65	0.16	130
	Tempe-Chryse-Acidalia-Deuteronilus/Cydonia Group	−3.91	0.08	0.94	−3.89	0.08	0.94	0.01	110
	Utopia-Astapus/Pyramus-Elysium Group	−3.58	0.09	1.11	−3.66	0.08	1.20	0.13	140
Other Landforms	Chan et al., 2018 – Valley Network Termini	−1.70	0.81	4.18	−1.70	0.81	4.18	0.00	740
	Di Achille and Hynek, 2010 – Open Basin Deltas	−2.54	0.18	0.65	−2.54	0.17	0.64	0.06	440
	Updated Open Basin Deltas	−2.29	0.43	1.38	−2.27	0.42	1.33	0.09	510

Expanding the deformation modeling to the entirety of the Carr and Head (2003) mapped Arabia Level shows that there is still high variance within the paleotopography. For this level definition, the mean elevation drops from -2.31 ± 1.30 km to -2.53 ± 1.11 km pre-Tharsis, with topographic ranges of 6.13 km and 5.71 km respectively. A better fit is achieved by removing the Isidis data points, resulting in a mean paleoelevation of -2.39 ± 0.84 km and range of 4.21 km, but this is still not an equipotential surface.

To account for the possibility that different parts of the Carr and Head (2003) Arabia Level may have formed at different times and/or by different formational processes, the level was split into eight segments: Memnonia, Tempe, Chryse, Deuteronilus, Nilosyrtis, Isidis, Amenthes, and Nepenthes (Fig. 1). This segmentation optimizes each one for C (percentage of Tharsis built at time of level emplacement).

Half of these segments are optimized similarly to Arabia Terra segment with $C = 1$ suggesting a best-fit scenario of pre-Tharsis rise formation and with similar $\sigma_{r.m.s.}$ values (ranging from 0.41 km to 0.89 km). However, the other half (Nilosyrtis, Isidis, Amenthes, and Nepenthes) were best fit to values of $C = 0$ suggesting that *if* they were shoreline segments they would have formed after the Tharsis rise complex. These segments also have similar $\sigma_{r.m.s.}$ values ranging from 0.27 km to 1.05 km. Additionally, the segments closest to the Tharsis bulge (Memnonia, Tempe, Chryse, and Deuteronilus) had noticeable decreases in their standard deviation between the modern and paleotopography, while those closer to the antipodal bulge (Nilosyrtis, Isidis, Amenthes, and Nepenthes) had their standard deviation increase within their paleotopography.

Comparisons of all the global Arabia Level definitions Sholes et al. (2021) shows that while some of the long-wavelength trend is removed, the overall long- and short-wavelength scatter across the data is still present (Fig. 2). While most levels had a decrease in the standard deviation between their modern- and paleoelevation data, from 0 to 40%, the values still remain over 700 m (with the exception of the small regional mappings). Additionally, the mean paleoelevation for each of the levels spans 1.8 km; ranging from the Webb (2004) regional mapping at −3.47 km up to −1.69 km for the original Parker et al. (1989) without Isidis.

The Arabia Level definitions show a wide diversity of C values ranging from 1.0 (suggesting a best-fit scenario of pre-Tharsis rise formation) to 0.16 (suggesting a late-stage level formation relative to Tharsis). The average C value for all tested global and regional maps is 0.64 ± 0.25 which decreases to 0.56 ± 0.25 when removing the circum-Isidis data. Overall, the best-fit model curves for each of the level definitions present drastically different and ranged timing scenarios throughout the rise of Tharsis.

In particular, minimizing the $\sigma_{r.m.s.}$ for the Clifford and Parker (2001) mapped level gives a value of $C = 0.57$ ($\sigma_{r.m.s.} = 1.07$ km; without Isidis: $C = 0.75$, $\sigma_{r.m.s.} = 0.95$ km). This suggests that the original mapped data that was used to create the digitized Carr and Head (2003) level and adopted in the geophysical deformation models has a much younger formational time than those model results ($C = 1.0$). The topography of this original data (Clifford and Parker, 2001), based on the geological context within the *Viking* images, has a modern day mean elevation of -2.23 ± 1.25 km and a topographic range of 6.86 km. While the best-fit mean paleoelevation is -2.19 ± 1.07 km has a smaller $\sigma_{r.m.s.}$, the total topographic range increases to 7.14 km (-2.07 ± 0.95 km and range of 5.96 km when excluding the Isidis region).

The smaller regional detailed mappings of the Cydonia Mensae and Deuteronilus Mensae regions also have best-fit values of C in the range of 0.16–0.52 suggesting that if these features are valid shorelines, they would have formed during the early-to-middle stages of Tharsis' emplacement rather than prior to it. The Sholes et al. (2021) mapping was done based on the original Parker et al. (1989) level definitions and was shown to differ by more than 500 km from the levels used by the previous geophysical deformation modelling studies. The large discrepancy between the values of C between the original defined

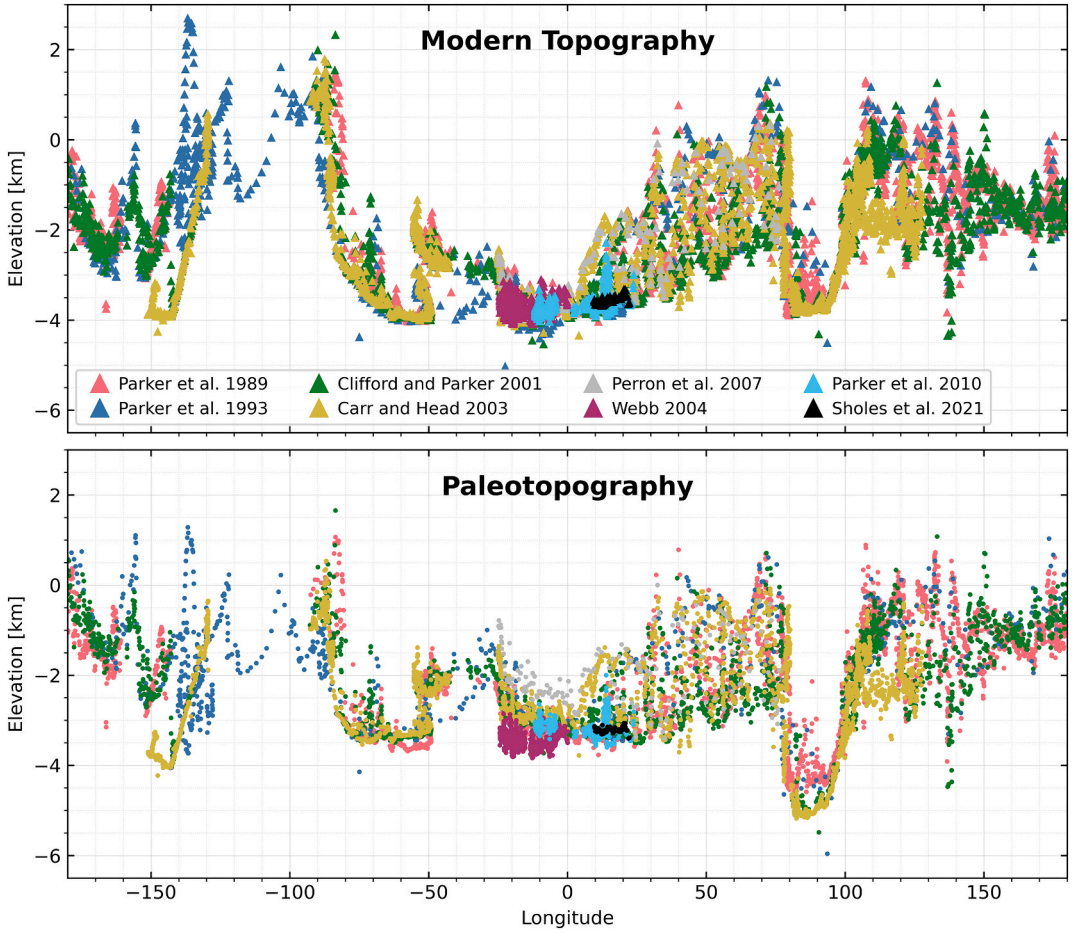

Fig. 2. Comparisons of the topographic scatter in the modern (top) and best-fit paleotopography (bottom) of the different Arabia Level mappings. See Table 1 for best-fit parameters of each map/mapping.

mapped level and that of those used in the models, raises more doubt on their validity as ocean paleoshorelines.

4.2. *Deuteronilus level*

We also applied the TID model to the better defined Deuteronilus Level, specifically using the higher resolution mapped geospatial data from Ivanov et al. (2017) (Fig. 3). These data were originally mapped in nine different regions in the northern plains: Tempe, Chryse, Acidalia, Deuteronilus/Cydonia, Astapus/Pyramus, Utopia, Western Elysium, Phlegra, and Tantalus (the Isidis basin was also mapped, but was determined to post-date the VBF in the northern plains). The authors applied the Perron et al. (2007) TPW model to the data and found that the features best fit two distinct topographic levels: the Tempe-Chryse-Acidalia-Deuteronilus/Cydonia region (hereafter referred to as the Tempe Group) and the Astapus/Pyramus-Utopia-Wester Elysium region (hereafter referred to as the Utopia Group). The Phlegra and Tantalus regions were excluded from the paleotopography analysis as they likely experienced post-VBF changes in their regional topography, e.g., a topographic bulge associated with a graben swarm in Tantalus Fossae. But application of the TID by Citron et al. (2018) focused on the global Deuteronilus Level without considering the possibility that these features represented two (or more) possible different levels.

Our global application of the TID model agrees with the results of Citron et al. (2018) with a best fit mean paleoelevation of -3.68 ± 0.11 km and C = 0.16 indicating late-stage development relative to Tharsis. Note that there are some small differences in values between studies are due to the use of different topographic data, i.e., MOLA 4 ppd. gridded data versus the MOLA/HRSC blended data used here. When fitting the TID model to the two Ivanov et al. (2017) regions, the Tempe Group has a best-fit paleo mean elevation of -3.89 ± 0.08 km, with $C = 0.01$, and the Utopia group has a best-fit mean elevation of -3.66 ± 0.08 km, with $C = 0.13$ (Tharsis 99% and 87% complete respectively). These are both best-fit to late-stage development of Tharsis (both later than the combined global level) with the Tempe Group best-fit to having little to no influence from the rise of Tharsis. The $\sigma_{r.m.s.}$ for each of these groups is smaller than that of the global level.

There is a possibility that the many mapped sections may represent different possible levels, either separately or in different groups. However, there is geomorphological continuity and crater count ages to suggest that the features formed at roughly the same time (Ivanov et al., 2017). We did find the best-fit relative ages for every possible combination of the nine segments (forming 1 to 9 groups) and the smallest total $\sigma_{r.m.s.}$ (of 0.06) was with five groups: Astapus/Pyramus ($C = 0.16$), Western Elysium ($C = 0.56$), Acidalia-Chryse-Deuteronilus/Cydonia-Phlegra-Tempe ($C = 0$), Utopia ($C = 0.14$), and Tantalus ($C = 0.18$). However, this analysis is likely skewed and inaccurate as the approximate maximum surface resolution of the degree-5 spherical harmonics is ~2,100 km which is greater than all but the Astapus/Pyramus segment (with Western Elysium the smallest at ~550 km long), which can lead to overfitting especially if other regional topographic processes have deformed the features (e.g., Tantalus). Thus, we defer to the Tempe and Utopia Groups proposed by Ivanov et al. (2017) which have topographic and geomorphic continuity, similar ages of ~3.6 Ga, and relatively small best-fit $\sigma_{r.m.s.}$.

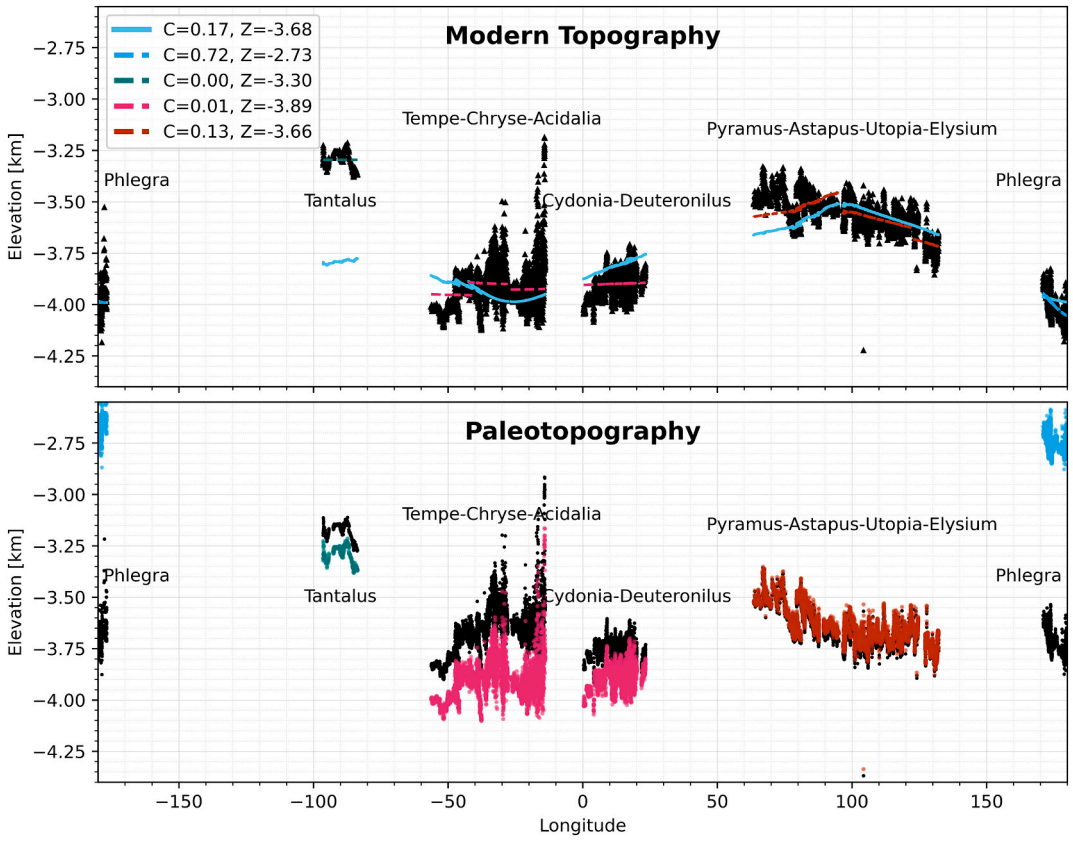

Fig. 3. Modern (top) and best-fit paleotopography (bottom) for the Ivanov et al. (2017) mapped Deuteronilus Level. *Top)* Black dots show the modern topography of the level. Solid blue curves note the best-fit model using the Citron et al. (2018) parameters (for *C*, percentage of Tharsis buildup, and *Z*, mean elevation or 'sea level'). Colored curves (and corresponding paleotopography points) indicate best-fit TID model results to the individual sections (Tantalus is green, Phlegra is blue, the Tempe Group is magenta, and the Utopia Group is orange). *Bottom*) Black dots represent the paleotopography of the level using the parameters from Citron et al. (2018). For completeness, the Phlegra and Tantalus sections have been optimized to their own best-fit paleotopography here, but these segments are small (relative to the resolution of the spherical harmonics used), discontinuous to the other segments, and likely were deformed by other regional processes (see text). (For interpretation of the references to colour in this figure legend, the reader is referred to the web version of this article.)

4.3. Dichotomy deltas and valley networks

Fig. 4 shows the relative modern and paleoelevation positioning between the open-bain deltas, valley-network termini, and the Carr and Head (2003) putative shoreline data. There is no significant change between the modern and paleoelevations of the open-basin deltas presented in Di Achille and Hynek (2010) (-2.54 ± 0.18 km paleotopography), however the best-fit value for *C* is 0.06, suggests emplacement at the very end of the Tharsis rise. The updated list of open basin deltas from Rivera-Hernandez and Palucis (2019) provides a similar timeframe ($C = 0.09$) but the $\sigma_{r.m.s.}$ for the data is more than double (paleoelevation of -2.27 ± 0.42 km). These mean paleoelevations are also ~900 m higher in elevation than the mean elevations of the more detailed regional level mappings.

The valley-network termini data from Chan et al. (2018) are found to have a best-fit value of $C = 0$ which is, in general, counter to their results. This is likely the result of their primary use of the TPW model and testing the TID model using the *C* parameters obtained by Citron et al. (2018) from fitting the Arabia Terra level segment. These results suggest that if the valley network termini do indeed represent marine-adjacent features from the same erosional time period, they would have formed sometime after the completion of Tharsis' growth. The optimized mean paleoelevation is comparable to some of the early Parker et al. studies sans-Isidis region but ~1.5 km higher in elevation from the mean paleoelevations of the detailed regional studies (Parker et al., 2010; Sholes et al., 2021; Webb, 2004).

5. Discussion

While the geophysical deformation models are able to account for some of the long-wavelength trends of their tested putative paleoshoreline segment in Arabia Terra, we have shown that their ability to do so is highly sensitive to the location of the input features (i.e., which paleoshoreline level definition is used). Sholes et al. (2021) showed that this tested Arabia Level segment varied drastically, in places more than 500 km, from the geomorphological contact used to originally define the putative paleoshoreline. Thus, not only are the data used in these models inaccurate, but our testing of different maps, mappings, and individual segments of the levels gives a wide range of values for the timing, placement, and magnitude of any ancient martian oceans. Nearly all tested global and segmented regions for the Arabia Level had worse root-mean-square errors than presented in the literature.

A large potentially problematic issue with these geophysical deformation model studies is the lack of characterization of the paleotopography itself. For most features analyzed, the deviation and total range within each level's paleotopography are relatively comparable to their modern values (Fig. 5, Table 1). Thus, by extension, if the levels' large topographic range and dispersion in their modern elevation precludes their interpretation as possible shorelines (e.g., Carr and Head, 2003; Sholes et al., 2021), then the same can be concluded from the observed large topographic range and dispersion found within the paleotopography. And while the modeled deformation curve may generally follow the overall trend of the elevation data, the overall distribution and shape of the actual paleotopography is nearly identical to the modern data

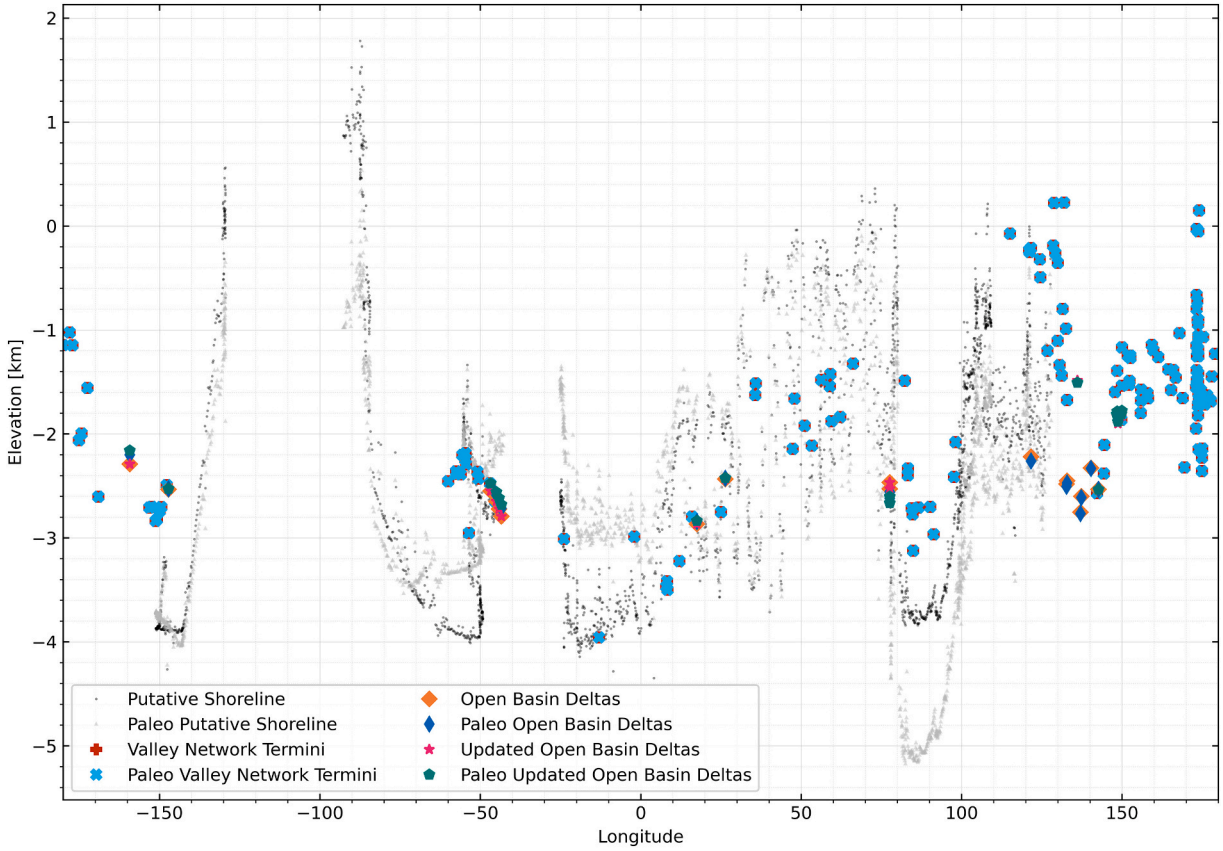

Fig. 4. Modern and best-fit paleoelevations for other putative ocean landforms. Valley network termini (Chan et al., 2018), open-basin deltas (Di Achille and Hynek, 2010), Arabia Level putative paleoshoreline (Carr and Head, 2003), and updated open-basin deltas (this study) are shown.

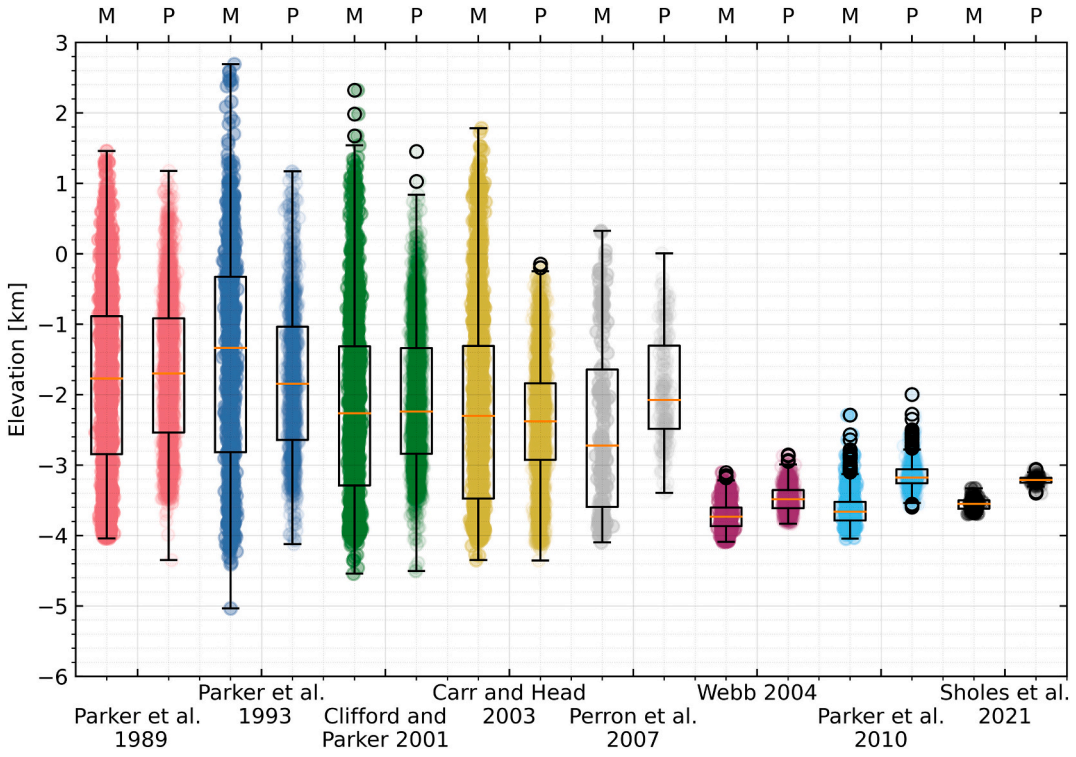

Fig. 5. Box-and-Whisker plot showing the variance in the different Arabia Level maps for both the modern (M) and paleotopography (P). These are the data without the inclusion of Isidis (see text). Artificial jitter is introduced to separate out the individual points. Even when correcting for deformation due to Tharsis, there is still multiple kilometers of the range of the putative paleoshoreline.

(Fig. 2). For the Arabia Level, neither the modern- nor paleotopography constitute an equipotential surface.

There is also considerable disagreement on the timing of each of the putative paleoshorelines based on the TID modeling results. Optimizing the scaling parameter *C,* for percentage of Tharsis built after feature emplacement, runs nearly the full parameter space ($C = 0.16$ to 1) for the Arabia Level mappings which suggest that, without a standardized detailed global mapping for the level, the TID model is unable to constrain the timing relative to the rise of Tharsis. Furthermore, whether the outlying data surrounding the Isidis basin is included or not gives inconsistent timing results and a positive geoid anomaly over Isidis suggest that additional loading occurred sometime after its formation (Ritzer and Hauck II, 2009) which may have further deformed the levels (Citron et al., 2021).

The best-fit scaling parameters optimized for the global Deuteronilus Level and the two Ivanov et al. (2017) groups show similar disagreement and highlight another potential limitation of the models. For example, while the global contact has a best-fit timing of $C = 0.16$ (Tharsis 84% complete), optimizing the level for each of the proposed segment groups gives varying results with the Tempe Group having a $C = 0.01$ and the Utopia Group best fit to $C = 0.13$ but having different mean paleoelevations vertically offset by approximately 230 m (~3× the standard deviation). Since both levels occupy the same basin and have equivalent timing parameters, either the features were formed at very close intervals at very different elevations or there is a deficiency within the models itself (Citron et al., 2019). These results are heavily dependent on the base assumption that the levels are indeed shorelines and are expected to have been formed at an equipotential surface, which may not be the case for other proposed genetic origins.

We propose that the misalignment observed in the proposed paleoshoreline topography may simply be the result of misinterpreted features that fall along the topographic dichotomy itself. In other words, maps of the Arabia Level do not trace out paleoshorelines but generally track the topographic dichotomy where the slope is relatively steeper. So small deviations in the mapping of the features results in greater topographic divergence, compared for example the relatively flat northern plains the Deuteronilus Level occupies. The dichotomy itself may be the result of a large ancient impactor (Andrews-Hanna et al., 2008). This can explain why the geophysical deformation models are able to capture some of the general long-wavelength trends of the putative paleoshorelines but the paleotopography itself shows continued misalignment and scatter. This interpretation is also in agreement with the lack of positive identification of any marine shoreline morphology (e.g., Ghatan and Zimbelman, 2006; Malin and Edgett, 1999; Sholes et al., 2019) or mineralogy (e.g., Bibring et al., 2006) and the clear lack of an established global contact, feature, or map for the Arabia Level (Sholes et al., 2021). Thus, any observed long-wavelength trends are those of the topographic dichotomy, which itself would have been modified by the rise of Tharsis, and the observed short-wavelength scatter is the resulting noise caused by cross-cutting the surface topography and lateral uncertainty in their placement along the relatively steep dichotomy.

The different lines of evidence that have been used to support past oceans on Mars are also problematic. Assessing the paleotopography for the open-basin deltas, valley network termini, and putative paleoshorelines gives variable results for both the proposed elevation and timing of the hypothesized ancient oceans. TID modeling results for the open-basin deltas and valley network termini suggest formation after or during the very late-stages of Tharsis' growth and an elevation range inconsistent with an equipotential surface (both in the modern and paleotopography). This late-stage formation contradicts the general timing of the proposed Noachian-aged Arabia level ocean and the spread of timing values, *C*, for the proposed paleoshorelines (and their geographic locations are inconsistent with the younger Deuteronilus Level).

These large discrepancies in the modeled relative ages makes it difficult to reconcile all three lines of evidence into a coherent ocean scenario for Mars. Since the proposed paleoshorelines are not at an equipotential, the geophysical deformation models have been proposed to rectify the long-wavelength trends. Therefore, if the open-basin deltas and valley network termini were also formed at the margins of this proposed ancient ocean, they too would be subject to the same deformation. Yet, the results of this study show much inconsistency between each other and paleotopography data fails to provide support for an ancient ocean. The mean paleoelevations of each line of evidence further supports this view as does the relatively large standard deviations for each. Additionally, more detailed high-resolution regional analyses of these hypothesized features may continue to show non-support for a marine origin (De Toffoli et al., 2021; García-Arnay and Gutiérrez, 2020; Rivera-Hernandez and Palucis, 2019).

Interestingly, a subset of the dichotomy open basin deltas are located in Gale and Jezero crater, the sites of the *Curiosity* and *Perseverance* rovers respectively. Detailed mapping with orbital imagery and topography have revealed that these deltas formed in paleolake basins (e.g., Goudge et al., 2015; Palucis et al., 2016), with little geomorphic evidence to indicate that it they were ever connected to a northern ocean.

Attempts have been made to constrain the age of an Arabia Level ocean using both the geophysical deformation models and observed geomorphology of these two fluvial-lacustrine systems along the proposed level (Baum et al., 2021; Citron et al., 2021). For example, Jezero crater's well-preserved valley network and deltaic system show no observed modification by marine processes. If the paleotopography around the system would completely submerge the crater at a particular ocean level, then the ocean would have to predate the fluvial-lacustrine activity (Baum et al., 2021). However, these studies assume a fixed sea level, but as shown here and in Sholes et al. (2021), there is a high-degree of equivocalness in their placement and elevation (Sholes, 2022). This assumption of a fixed mean sea level ignores the reality of the 1-sigma standard deviation within the level which exceeds 1.1 km. Furthermore, accounting for the relatively younger (Ivanov et al., 2017) post-basin loading within Isidis causes Jezero to be situated above the mean sea level precluding its usefulness in relative age dating the proposed ocean (Citron et al., 2021). This high-degree of uncertainty with the location, and by extension paleoelevation, of the Arabia Level precludes the effectiveness of such studies in age-dating such an ocean and highlights the dependence on model used, choice of putative shoreline mapping, and validity of those mapped features as true paleoshorelines.

The amount of water that these proposed ocean levels could hold at their mean paleoelevations are all within the same order of magnitude, several hundreds of meters global equivalent layer (GEL), due to the relative flatness of the northern plains. However, these values are generally much greater than past volume estimates of 25–240 m GEL allow for (e.g., Carr and Head, 2015; Villanueva et al., 2015). Scheller et al. (2021) suggest a greater initial water volume of 100–1500 m GEL largely due to subsequent sequestration via irreversible chemical weathering (i.e., crustal hydration). Similarly, Chassefière et al. (2013) used a simple model to show that ~500 GEL of water could be stored through early serpentinization reactions as subsurface serpentine. Scheller et al. (2021)'s preferred model has an initial water volume of 570 GEL which can support most of the global Arabia Level best-fit ocean volumes in the early Noachian, but sharply declines to ~100 GEL by the start of the Hesperian which is incompatible with all our modeled ocean volumes. This preferred model though is incompatible with a Hesperian-aged ocean (e.g., Deuteronilus Level) which requires >100 GEL of surface liquid water.

6. Conclusion

Geophysical deformation models have been suggested by previous studies to explain the observed multi-kilometer range of elevations observed in proposed ocean paleoshorelines on Mars (Citron et al., 2018; Perron et al., 2007). However, these studies applied these models on smaller and potentially inaccurate segments of the Arabia and

Deuteronilus Levels. Our work builds upon these studies by applying their models to the Deuteronilus Level and to different definitions of the Arabia Level, considering the entirety of the levels as well as individual segments. Our results, show that the choice of level mapping can drastically change the paleotopography and therefore the model fit. This can lead to inaccurate estimates on the timing of such oceans, the magnitude of water required, and choices of paleosea level.

Our global analysis of the different proposed mappings of the Arabia Level show that the paleotopography of each feature does not constitute an equipotential surface. Not only is there still multi-kilometer short-wavelength scatter (over 10s-100s of degrees longitude), but there are still long-wavelength trends present within the paleotopography. Furthermore, inclusion of other lines of evidence into these models, namely the valley network termini and open-basin deltas, give highly-conflicting results with those of the Arabia and Deuteronilus Levels both in the magnitude and timing of such oceans.

These highly equivocal results show that the geophysical deformation models are not the catchall answer to explain the topographic disparity present in the proposed Mars paleoshoreline data. While this continues to cast doubt on the interpretation of the Arabia and other levels as ancient shorelines, this does not preclude the existence of past martian oceans. Furthermore, future work that analyzes such ancient features will need to account for the effects of the Tharsis rise on the shape and geoid of Mars while also showing internal consistency between multiple lines of evidence.

Declaration of Competing Interest

None.

Acknowledgments

We graciously thank Robert Citron sharing the geophysical deformation model along with Taylor Perron and Mikhail Ivanov for sharing their putative shoreline vector data. We also thank Mark Baum and an anonymous reviewer for their helpful comments that improved the clarity of the manuscript. This work was partially carried out by S.F.S. at the Jet Propulsion Laboratory, California Institute of Technology, under a contract with the National Aeronautics and Space Administration (80NM0018D0004).

The geophysical deformation code used is available at https://www.github.com/sfsholes/mars-deformation and archived on Zenodo at https://www.doi.org/10.5281/zenodo.6015512. .

References

Anderson, R.C., Dohm, J.M., Golombek, M.P., Haldemann, A.F., Franklin, B.J., Tanaka, K.L., et al., 2001. Primary centers and secondary concentrations of tectonic activity through time in the western hemisphere of Mars. J. Geophys. Res. 106 (E9), 20563–20585. https://doi.org/10.1029/2000JE001278.

Andrews-Hanna, J.C., Zuber, M.T., Banerdt, W.B., 2008. The Borealis basin and the origin of the martian crustal dichotomy. Nature 453 (7199), 1212–1215. https://doi.org/10.1038/nature07011.

Banerdt, W.B., Golombek, M.P., Tanaka, K.L., 1992. Stress and tectonics on Mars. In: Kieffer, H.H., Jakosky, B.M., Snyder, C.W., Matthews, M.S. (Eds.), Mars. The University of Arizona Press, Tucson, AZ, pp. 249–297.

Baum, M., Wordsworth, R., Goudge, T.A., 2021. Consequences of proposed shoreline deformation scenarios for Jezero Crater, Mars. Planet. Sci. J. 2 (4), 128. https://doi.org/10.3847/PSJ/ac01de.

Bibring, J.-P., Langevin, Y., Mustard, J.F., Poulet, F., Arvidson, R., Gendrin, A., et al., 2006. Global mineralogical and aqueous mars history derived from OMEGA/Mars express data. Science 312 (5772), 400–404. https://doi.org/10.1126/science.1122659.

Bouley, S., Baratoux, D., Matsuyama, I., Forget, F., Séjourné, A., Turbet, M., Costard, F., 2016. Late Tharsis formation and implications for early Mars. Nature 531 (7594), 344–347. https://doi.org/10.1038/nature17171.

Carr, M.H., Head, J.W., 2003. Oceans on Mars: an assessment of the observational evidence and possible fate. J. Geophys. Res. 108 (E5), 5042. https://doi.org/10.1029/2002JE001963.

Carr, M.H., Head, J.W., 2010. Geologic history of Mars. Earth Planet. Sci. Lett. 294 (3–4), 185–203. https://doi.org/10.1016/j.epsl.2009.06.042.

Carr, M.H., Head, J.W., 2015. Martian surface/near-surface water inventory: sources, sinks, and changes with time. Geophys. Res. Lett. 42 (3), 726–732. https://doi.org/10.1002/2014GL062464.

Carr, M.H., Head, J.W., 2019. Mars: formation and fate of a frozen Hesperian ocean. Icarus 319, 433–443. https://doi.org/10.1016/j.icarus.2018.08.021.

Cattermole, P., 1992. The evolution of Tharsis. In: Mars: The Story of the Red Planet. Chapman & Hall, London, pp. 183–189.

Chan, N.H., Perron, J.T., Mitrovica, J.X., Gomez, N.A., 2018. New evidence of an ancient Martian ocean from the global distribution of valley networks. J. Geophys. Res. 123 (8), 2138–2150. https://doi.org/10.1029/2018JE005536.

Chassefière, E., Langlais, B., Quesnel, Y., Leblanc, F., 2013. The fate of early Mars' lost water: the role of serpentinization. J. Geophys. Res. 118 (5), 1123–1134. https://doi.org/10.1002/jgre.20089.

Citron, R.I., Manga, M., Hemingway, D.J., 2018. Timing of oceans on Mars from shoreline deformation. Nature 555 (7698), 643–646. https://doi.org/10.1038/nature26144.

Citron, R.I., Manga, M., Hemingway, D., Keane, J., 2019. Early Martian oceans: geophysical constraints from shoreline deformation models. In: Paper presented at the 9th International Conference on Mars, Pasadena, CA.

Citron, R.I., Manga, M., Hemingway, D., Plattner, A., 2021. Are we visiting the coastlines of Mars? Load-corrected paleo-ocean levels at Jezero, Oxia Planum, and Gale. In: Paper presented at the 52nd Lunar and Planetary Science Conference, 1605.

Clifford, S.M., Parker, T.J., 2001. The evolution of the Martian hydrosphere: implications for the fate of a primordial ocean and the current state of the northern plains. Icarus 154 (1), 40–79. https://doi.org/10.1006/icar.2001.6671.

Daradich, A., Mitrovica, J.X., Matsuyama, I., Perron, J.T., Manga, M., Richards, M.A., 2008. Equilibrium rotational stability and figure of Mars. Icarus 194 (2), 463–475. https://doi.org/10.1016/j.icarus.2007.10.017.

Davis, J.M., Aranos, L., Dickeson, Z.I., Fawdon, P., 2021. The evolution of ancient fluvial systems in Memnonia Sucli, Mars: impact crater damming, aggradation, and a large, inner sea on the dichotomy? Earth Space Sci. Open Archiv. 35. https://doi.org/10.1002/essoar.10507725.1.

De Toffoli, B., Plesa, A.C., Hauber, E., Breuer, D., 2021. Delta deposits on Mars: a global perspective. Geophys. Res. Lett. https://doi.org/10.1029/2021GL094271 e2021GL094271.

Di Achille, G., Hynek, B.M., 2010. Ancient ocean on Mars supported by global distribution of deltas and valleys. Nat. Geosci. 3 (7), 459–463. https://doi.org/10.1038/ngeo891.

Dickeson, Z.I., Davis, J.M., 2020. Martian Oceans. Astron. Geophys. 61 (3), 3.11–13.17. https://doi.org/10.1093/astrogeo/ataa038.

Evans, A.J., Andrews-Hanna, J.C., Zuber, M., 2010. Geophysical limitations on the erosion history within Arabia Terra. J. Geophys. Res. 115 (E5) https://doi.org/10.1029/2009JE003469.

Fergason, R.L., Hare, T.M., Laura, J., 2018. HRSC and MOLA Blended Digital Elevation Model at 200m v2. USGS Astrogeology Science Center.

García-Arnay, Á., Gutiérrez, F., 2020. Reconstructing paleolakes in Nepenthes Mensae, Mars, using the distribution of putative deltas, coastal-like features, and terrestrial analogs. Geomorphology 359, 107129. https://doi.org/10.1016/j.geomorph.2020.107129.

Ghatan, G.J., Zimbelman, J.R., 2006. Paucity of candidate coastal constructional landforms along proposed shorelines on Mars: Implications for a northern lowlands-filling ocean. Icarus 185 (1), 171–196. https://doi.org/10.1016/j.icarus.2006.06.007.

Goudge, T.A., Aureli, K.L., Head, J.W., Fassett, C.I., Mustard, J.F., 2015. Classification and analysis of candidate impact crater-hosted closed-basin lakes on Mars. Icarus 260, 346–367. https://doi.org/10.1016/j.icarus.2015.07.026.

Head, J.W., Hiesinger, H., Ivanov, M.A., Kreslavsky, M.A., Pratt, S., Thomson, B.J., 1999. Possible ancient oceans on Mars: evidence from Mars Orbiter Laser Altimeter data. Science 286 (5447), 2134–2137. https://doi.org/10.1126/science.286.5447.2134.

Hynek, B.M., Beach, M., Hoke, M.R., 2010. Updated global map of Martian valley networks and implications for climate and hydrologic processes. J. Geophys. Res. 115 (E9) https://doi.org/10.1029/2009JE003548.

Ivanov, M.A., Erkeling, G., Hiesinger, H., Bernhardt, H., Reiss, D., 2017. Topography of the Deuteronilus contact on Mars: evidence for an ancient water/mud ocean and long-wavelength topographic readjustments. Planet. Space Sci. 144, 49–70. https://doi.org/10.1016/j.pss.2017.05.012.

Jaumann, R., Neukum, G., Behnke, T., Duxbury, T.C., Eichentopf, K., Flohrer, J., et al., 2007. The high-resolution stereo camera (HRSC) experiment on Mars Express: instrument aspects and experiment conduct from interplanetary cruise through the nominal mission. Planet. Space Sci. 55 (7–8), 928–952. https://doi.org/10.1016/j.pss.2006.12.003.

Leverington, D., Ghent, R., 2004. Differential subsidence and rebound in response to changes in water loading on Mars: possible effects on the geometry of ancient shorelines. J. Geophys. Res. 109 (E1) https://doi.org/10.1029/2003JE002141.

Malin, M.C., Edgett, K.S., 1999. Oceans or seas in the Martian northern lowlands: high resolution imaging tests of proposed coastlines. Geophys. Res. Lett. 26 (19), 3049–3052. https://doi.org/10.1029/1999GL002342.

Malin, M.C., Bell, J.F., Cantor, B.A., Caplinger, M.A., Calvin, W.M., Clancy, R.T., et al., 2007. Context camera investigation on board the Mars Reconnaissance Orbiter. J. Geophys. Res. 112 (E5), E05S04 https://doi.org/10.1029/2006JE002808.

Matsuyama, I., Manga, M., 2010. Mars without the equilibrium rotational figure, Tharsis, and the remnant rotational figure. J. Geophys. Res. 115 (E12) https://doi.org/10.1029/2010JE003686.

Melosh, H., 1980. Tectonic patterns on a reoriented planet: Mars. Icarus 44 (3), 745–751. https://doi.org/10.1016/0019-1035(80)90141-4.

Palucis, M.C., Dietrich, W.E., Williams, R.M., Hayes, A.G., Parker, T., Sumner, D.Y., et al., 2016. Sequence and relative timing of large lakes in Gale crater (Mars) after the formation of Mount Sharp. J. Geophys. Res. 121 (3), 472–496. https://doi.org/10.1002/2015JE004905.

Parker, T.J., Saunders, S.R., Schneeberger, D.M., 1989. Transitional morphology in West Deuteronilus Mensae, Mars: implications for modification of the lowland/upland boundary. Icarus 82 (1), 111–145. https://doi.org/10.1016/0019-1035(89)90027-4.

Parker, T.J., Gorsline, D.S., Saunders, R.S., Pieri, D.C., Schneeberger, D.M., 1993. Coastal geomorphology of the Martian northern plains. J. Geophys. Res. 98 (E6), 11061–11078. https://doi.org/10.1029/93JE00618.

Parker, T.J., Grant, J.A., Franklin, B.J., 2010. The northern plains: a Martian oceanic basin? In: Cabrol, N.A., Grin, E.A. (Eds.), Lakes on Mars. Elsevier, Boston, pp. 249–273.

Perron, J.T., Mitrovica, J.X., Manga, M., Matsuyama, I., Richards, M.A., 2007. Evidence for an ancient martian ocean in the topography of deformed shorelines. Nature 447 (7146), 840–843. https://doi.org/10.1038/nature05873.

Ritzer, J.A., Hauck II, S.A., 2009. Lithospheric structure and tectonics at Isidis Planitia, Mars. Icarus 201 (2), 528–539. https://doi.org/10.1016/j.icarus.2009.01.025.

Rivera-Hernandez, F., Palucis, M.C., 2019. Do deltas along the crustal dichotomy boundary of Mars in the Gale crater region record a northern ocean? Geophys. Res. Lett. https://doi.org/10.1029/2019GL083046.

Roberts, J.H., Zhong, S., 2004. Plume-induced topography and geoid anomalies and their implications for the Tharsis rise on Mars. J. Geophys. Res. 109 (E3) https://doi.org/10.1029/2003JE002226.

Roberts, J.H., Zhong, S., 2007. The cause for the north–south orientation of the crustal dichotomy and the equatorial location of Tharsis on Mars. Icarus 190 (1), 24–31. https://doi.org/10.1016/j.icarus.2007.03.002.

Ruiz, J., Fairen, A.G., Dohm, J.M., Tejero, R., 2004. Thermal isostasy and deformation of possible paleoshorelines on Mars. Planet. Space Sci. 52 (14), 1297–1301. https://doi.org/10.1016/j.pss.2004.06.003.

Scheller, E., Ehlmann, B., Hu, R., Adams, D., Yung, Y., 2021. Long-term drying of Mars by sequestration of ocean-scale volumes of water in the crust. Science 372 (6537), 56–62. https://doi.org/10.1126/science.abc7717.

Sholes, S.F., 2019. Geomorphic and Atmospheric Investigations on the Habitability of Past and Present Mars. Doctoral Degree. University of Washington, Seattle, WA.

Sholes, S.F., 2022. Were Jezero and Gale Craters submerged by a martian ocean? Quantified uncertainties in paleo-ocean levels on Mars. In: Paper presented at the 53rd Lunar and Planetary Science Conference.

Sholes, S.F., Catling, D.C., Pretlow, R., Montgomery, D.R., 2014. High-resolution examination of the geomorphology of proposed ocean shorelines on Mars. In: Paper Presented at the 8th International Conference on Mars, Pasadena, CA, p. 1014.

Sholes, S.F., Montgomery, D.R., Catling, D.C., 2019. Quantitative high-resolution reexamination of a hypothesized ocean shoreline in Cydonia Mensae on Mars. J. Geophys. Res. 124 (2), 316–336. https://doi.org/10.1029/2018JE005837.

Sholes, S.F., Dickeson, Z.I., Montgomery, D., Catling, D., 2021. Where are Mars' hypothesized ocean shorelines? Large lateral and topographic offsets between different versions of paleoshoreline maps. J. Geophys. Res. 126. https://doi.org/10.1029/2020JE006486.

Smith, D.E., Zuber, M.T., Frey, H.V., Garvin, J.B., Head, J.W., Muhleman, D.O., et al., 2001. Mars Orbiter Laser Altimeter: experiment summary after the first year of global mapping of Mars. J. Geophys. Res. 106 (E10), 23689–23722. https://doi.org/10.1029/2000JE001364.

Sohl, F., Spohn, T., 1997. The interior structure of Mars: implications from SNC meteorites. J. Geophys. Res. 102 (E1), 1613–1635. https://doi.org/10.1029/96JE03419.

Villanueva, G.L., Mumma, M.J., Novak, R.E., Käufl, H.U., Hartogh, P., Encrenaz, T., et al., 2015. Strong water isotopic anomalies in the martian atmosphere: probing current and ancient reservoirs. Science 348 (6231), 218–221. https://doi.org/10.1126/science.aaa3630.

Webb, V.E., 2004. Putative shorelines in northern Arabia Terra, Mars. J. Geophys. Res. 109 (E09010) https://doi.org/10.1029/2003JE002205.

Willemann, R.J., 1984. Reorientation of planets with elastic lithospheres. Icarus 60 (3), 701–709. https://doi.org/10.1016/0019-1035(84)90174-X.

Zuber, M.T., 2018. Oceans on Mars formed early. Nature 555, 590–591. https://doi.org/10.1038/d41586-018-03415-x.